

Distributed Deep Reinforcement Learning for Adaptive Medium Access and Modulation in Shared Spectrum

Akash Doshi and Jeffrey G. Andrews

Abstract

Spectrum scarcity has led to growth in the use of unlicensed spectrum for cellular systems. This motivates intelligent adaptive approaches to spectrum access for both WiFi and 5G that improve upon traditional carrier sensing and listen-before-talk methods. We study decentralized contention-based medium access for base stations (BSs) of a single Radio Access Technology (RAT) operating on unlicensed shared spectrum. We devise a learning-based algorithm for both contention and adaptive modulation that attempts to maximize a network-wide downlink throughput objective. We formulate and develop novel distributed implementations of two deep reinforcement learning approaches - Deep Q Networks and Proximal Policy Optimization - modelled on a two stage Markov decision process. Empirically, we find the (proportional fairness) reward accumulated by the policy gradient approach to be significantly higher than even a genie-aided adaptive energy detection threshold. Our approaches are further validated by improved sum and peak throughput. The scalability of our approach to large networks is demonstrated via an improved cumulative reward earned on both indoor and outdoor layouts with a large number of BSs.

Index Terms

Medium access, distributed reinforcement learning, contention, adaptive modulation, proportional fairness, decentralized partially observable Markov decision process, spectrum sharing

Akash Doshi and Jeffrey G. Andrews are with The University of Texas at Austin, TX 78712 (e-mail: akashsdoshi@utexas.edu, jandrews@ece.utexas.edu). This paper will be presented in part at the 55th Asilomar Conference on Signal, Systems and Computers, Nov. 2021 as an invited paper in the Session for Machine Learning in Communications [1]. This work was supported by the NSF under Grant CCF-2008710 and by NVIDIA.

I. INTRODUCTION

Unlicensed – or non-exclusively licensed – spectrum is set to play an increasing role in delivering broadband data traffic, both via WiFi and cellular standards-compliant systems. For example, over one GHz of bandwidth including the entire 6 GHz band was released for unlicensed use by the FCC in 2020. An early but still recent example of cellular use of unlicensed spectrum is the deployment of Long Term Evolution (LTE) in the unlicensed 5 GHz band, known as LTE-U, licensed-assisted access (LAA), and other proprietary names [2] [3], which allowed peak rates of advanced LTE devices to approach or even exceed 1 Gbps. Unlike licensed spectrum, access to unlicensed spectrum is free but regulated, for example by spectrum sensing technologies such as Listen-Before-Talk (LBT) [4] [5], which requires a transmitter to perform a Clear Channel Assessment (CCA) before accessing spectrum. The overarching goal of this paper is to apply state-of-the-art deep reinforcement learning tools to improve upon the state of the art in unlicensed spectrum access and rate adaptation.

A. Motivation and Application to 5G

Consider a BS attempting to decide whether or not the channel to one of its users (UEs) is sufficiently clear based on sensing the activity on the channel. As is well known, this spectrum sensing at the base station (BS) does not accurately reflect the quality of reception – measured in terms of the Signal-to-Interference plus Noise Ratio (SINR) – at the UE. Additionally, to a decision on whether to transmit or not, the BS uses adaptive modulation and coding (AMC) to optimize the rate and reliability for the current time slot based on recent channel conditions [6]. AMC does not usually take into account the change in interference pattern from the previous time slots, since a different set of transmitters may be activated every time slot. In this scenario, spectrum sensing provides the BS with at best partial knowledge of which other BSs are transmitting.

What is desirable and realistic is a medium access and AMC algorithm that is able to jointly process (i) information about reception quality at the UE from *previous* time slots and (ii) energy levels *currently* sensed at the BS. For (i), this information can be acquired using standard channel quality indicator (CQI) feedback as well as monitoring the throughput achieved to that UE, while (ii) is instantaneous information about the current interference state, but at the BS rather than the UE itself. Thus, this pairing of instantaneous and historical information should

be used collectively to jointly make both medium access and AMC decisions. A principled and effective mechanism for doing this is the main contribution of this paper.

To be concrete and timely, the model and algorithm in this paper is based on unlicensed spectrum access in 5G New Radio, known as NR-Unlicensed (NR-U). To transmit on shared spectrum in NR-U, a BS has to perform CCA for a randomized duration, which is determined by the category of LBT being utilized. We present an overview of the different categories in Section II-A. If a BS has chosen to transmit, it has to determine which Modulation and Coding Scheme (MCS) it will utilize. In NR, periodic UE feedback comprising of CQI, RSRP and RSRQ measurements [6], [7] are used by the BS to choose an MCS scheme from a lookup table, which is referred to as “inner loop” link adaptation [7]. “Outer loop” link adaptation [8] then utilizes received acknowledgements about successful UE packet decodes – ACK/NACK – to perform heuristic modifications to the estimated SINR. However, there is no framework for the BS to utilize information from CCA to aide the MCS lookup, or to incorporate CQI while determining whether or not to access shared spectrum. The algorithm we will design will enable the BS to jointly utilize both sources of information – spectrum sensing and UE feedback – to perform rate adaptation and determine medium access in shared spectrum.

B. Related Work

Several papers have attempted to utilize reinforcement learning to design a rule for choosing a transmit MCS. An online RL-based scheme for learning the best MCS scheme for a given SNR by interacting with the radio channel that can outperform look-up tables for AMC is designed in [9]. Subsequently, the authors of [9] extend their RL algorithm to a continuous state-space representation with a parameterized radial basis function (RBF) representation and also allow for interference in [10]. In [11], based on the knowledge of previous AMC decisions, an eNB uses tabular Q learning to adjust at run-time the MCS selection rules. All the algorithms outlined are single-agent RL algorithms that are not concerned with cooperative spectrum sharing or utilizing a contention-based access scheme. Moreover, none of these approaches utilize deep RL, and hence are not scalable to larger state spaces. More recently, a Deep Q Network (DQN) algorithm [12] for intelligent adaptive modulation by primary spectrum users in the face of imperfect spectrum sensing by secondary transmitters (STs) was designed in [13]. However, they do not optimize spectrum access of the primary spectrum users. Finally, in [14], the authors design a tabular Q learning algorithm for MCS selection that maximizes spectral efficiency

while maintaining low Block Error Rate (BLER) in a 5G setup. The algorithm designed in [14] outperforms inner and outer loop link adaptation, however it assumes full channel state information (CQI) and does not incorporate interference.

Recently, multi-agent reinforcement learning (RL) has been applied to design state-based policies that can improve the performance of unlicensed spectrum sharing [15]–[17]. In [18] and [17], they utilized deep Q -learning to either chose an action that adapts the ED threshold to the BS queue length or chooses the optimal subcarrier. Most recently, [19] presented a robust and scalable distributed RL design for radio resource management to mitigate interference. None of these papers thus far have attempted to model the asynchronous nature of the decisions made by the transmitters owing to contention. In [20], we developed a distributed deep RL spectrum sharing algorithm incorporating contention-based medium access. It deployed Deep Q Networks (DQN) at each BS that sequentially decide whether or not to transmit, with the goal of maximizing proportional fairness (PF) network-wide. In this paper, we provide a nontrivial generalization of [20], by expanding the action space of the BS from a simple yes/no transmit decision to a choice of modulation scheme, hence providing a framework for rate adaptation. Moreover, we propose modifications to the training algorithm, including the development of a new policy gradient based approach, that significantly improve the maximization of the proportional fairness metric from [20] and provide for scalability of the approach to more practical scenarios with a large number of BSs.

C. Contributions

We design novel distributed implementations of two single-agent reinforcement learning algorithms, adapted to a contention-based medium access *DEC-POMDP*, that can choose the optimal transmit modulation scheme at the BS in every time slot with the objective of maximizing the proportional fairness of UE throughput. Our technical contributions are three-fold.

Incorporating Adaptive Modulation into a RL framework for a Medium Access *DEC-POMDP*: We formulate adaptive medium access and modulation for BSs accessing shared spectrum as a *DEC-POMDP* with a novel reward structure adapted to an action space comprising of a choice of seven modulation schemes, including cross QAMs [21], ranging from QPSK to 256-QAM. The reward utilized is a function of the symbol error rate and received modulation scheme at each UE, and provides for long term PF of throughput delivered to the UEs. We then exploit the inter-BS energies detected during contention as inter-agent messaging [22] and add

recurrency to design novel multi-agent adaptations of two single agent RL algorithms – DQN [12] and Proximal Policy Optimization (PPO) [23]. The RL algorithms designed perform rate adaptation at the BS, by modifying the RL loss functions to incorporate the 2 stage MDP arising from contention-based spectrum access.

Superior performance versus genie-aided baselines: The proposed decentralized RL algorithms accumulate a significantly higher PF metric than both a standard ED = -72 dBm threshold as well as a genie-aided centralized Adaptive ED threshold, and subsequently increase the UE sum rate by $\sim 35\%$ over the Adaptive ED baseline. The RL algorithms train a policy at each BS that chooses a modulation scheme by considering both UE signalling parameters from the previous time slot as well as spectrum sensing information from the current time slot, and hence perform well in a wide variety of scenarios, unlike the ED = -72 dBm threshold that is based solely on spectrum sensing.

Improved Scalability of the proposed RL framework: We highlight the applicability of our results to relatively large 3GPP layouts: one indoor with 12 BSs and the other outdoor with 19 BSs. This is a significant improvement in scalability over [20] which had only 4 BSs, as well as other recent works utilizing multi-agent RL for cognitive radio [18], [19] which utilize under ten BSs and only perform adaptive medium access, not modulation. The rapid training convergence, low training sample complexity and the significant performance improvement over genie-aided non-ML baselines can be attributed to the *decentralized actor centralized critic* approach we employ to learn a RL policy at each BS.

The paper is organized as follows. In Section II, we describe the system model and provide a mathematical formulation for adaptive modulation at the BS to maximize proportional fairness. A brief overview of the DEC-POMDP formulation for contention-based medium access, adapted to adaptive modulation is provided in Section III, followed by a detailed exposition of the RL techniques used to solve the DEC-POMDP in Section IV. The simulations and detailed results are presented in Section V and VI respectively, followed by the conclusions and possible future directions in Section VII.

II. PROBLEM STATEMENT AND SYSTEM MODEL

A. Model Overview

We consider a downlink cellular deployment of N BSs, with a single UE scheduled per time slot per BS. We do not consider the problem of UE scheduling in this paper and assume that it

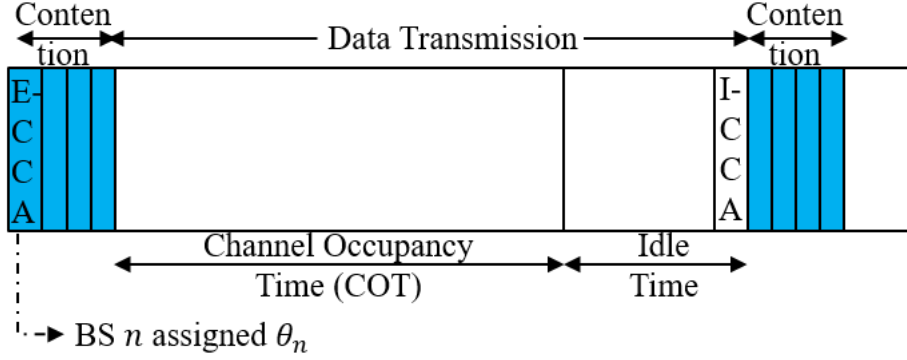


Fig. 1. Contention-based spectrum access model adopted in this paper, based on NR-U [24]

is provided by a higher layer entity. We assume that the DL transmission for all BSs occurs on the same sub-band of shared unlicensed spectrum, while the error-free reporting of DL CQI in the uplink (UL) occurs on separate licensed sub-bands, as in LAA. With the same UE scheduled at a given BS for L consecutive time slots, the medium access control (MAC) algorithm at the BS has to determine whether or not to transmit in each time slot, and if it chooses to transmit, which modulation scheme to use.

The procedure for performing CCA in NR-U is depicted in Fig. 1. In systems where data is transmitted in time slots of fixed length, referred to as Frame Based Equipment (FBE) by [5], each time slot is divided into a contention period and a data transmission phase. The data transmission phase typically consists of a period when the UE receives data (COT in Fig. 1) and an idle phase. The length of the idle phase depends on the nature of traffic received, varying from zero in case of full-buffer traffic to most of the data transmission phase in case of bursty XR traffic. The length of the contention period is determined by the category of LBT in NR-U [24]:

- In Category 1 (Cat 1) LBT, there is no contention.
- In Category 2 (Cat2) LBT, the BS would merely sense the channel for a fixed period of time at the end of a data frame, denoted by I-CCA (Initial CCA) in Fig. 1, and if it remained idle (based on the ED threshold), the BS transmitted data for a fixed time period (a maximum of 9 ms) and then sensed the channel again.
- Category 3 and 4 (Cat3 and Cat4) LBT are later variants, that introduced an extended CCA period (E-CCA) in which a BS senses the channel for a further random duration if

the channel remained idle during I-CCA. To determine this random duration, henceforth referred to as the ‘‘Contention’’ phase, a BS will draw a random counter θ between 0 and $\text{CWS} - 1$ (where CWS denotes the contention window size e.g. $\text{CWS} = 4$ in Fig. 1). It will then decrement θ by 1 every $5 \mu\text{s}$, and transmit after θ hits 0 only if the channel remained idle for the entire duration.

In this paper, we adopt a contention-based channel access scheme that is a simplified version of Cat3 LBT in NR-U [24] for full buffer data transmission. We allow for counter collisions i.e. $\theta_i = \theta_j$ for $i \neq j$. Moreover, if BS i chooses to transmit when θ_i hits 0, it transmits a unique orthogonal preamble for the remainder of the contention phase followed by data from the beginning of the data transmission phase. The objective of each BS is to choose the modulation scheme in each time slot which maximizes the long term UE throughput. We now formulate this mathematically.

B. Mathematical Formulation

Assume each BS has a set of K modulation schemes $M = \{M_1, M_2 \dots M_K\}$ to choose from. Denote the modulation scheme chosen by BS i to transmit to UE i by m_i . For example, $m_i = 16$ implies BS i utilizes 16 QAM to transmit. Subsequently, we can define $s_i \in S_i$ as the symbol transmitted by BS i , where

$$S_i = \{x_k\}_{k \in [m_i]} \text{ where } x_k \in m_i \text{ QAM.} \quad (1)$$

Considering single-input single-output (SISO) communication between BSs and UEs in a single sub-band, we denote the channel between the BS i and UE j by h_{ij} , and the channel between BS i and BS j by h'_{ij} where i and j are drawn for $i, j \in \{1, \dots, N\}$. The respective power gains are $g_{ij} = |h_{ij}|^2$ and $g'_{ij} = |h'_{ij}|^2$. For each BS i , $a_i \in \{0, 1\}$ denotes whether the BS chose to transmit or not, with transmission denoted by 1. For each UE j , S_j denotes the desired signal power, I_j the total interference power, R_j the data rate experienced and \bar{X}_j the exponentially smoothed average rate seen by the UE, with the vector containing these terms for all UEs being denoted by \mathbf{S} , \mathbf{I} , \mathbf{R} and $\bar{\mathbf{X}}$ respectively. Denote the noise variance for DL receptions at the UE by σ_{UE}^2 , and at the BS by σ_{BS}^2 .

Consider transmissions on a DL slot from BSs to UEs. Assuming a BS i , with transmit decision given by a_i , transmits symbol s_i at a constant power ρ , the received symbol y_j at each

UE j is given by

$$y_j = \sqrt{\rho}h_{jj}s_ja_j + \sum_{i \neq j} \sqrt{\rho}h_{ij}s_i a_i + z_j, \quad (2)$$

where $z_j \sim \mathcal{CN}(0, \sigma_{\text{UE}}^2)$, with \mathcal{CN} denoting the complex normal distribution and σ_{UE}^2 the noise variance at the UE. Then the SINR measured at UE j at the end of data transmission in time slot n is given by

$$\text{SINR}_j[n] = \frac{g_{jj}[n]\rho a_j[n]}{\sigma_{\text{UE}}^2 + \sum_{i=1, i \neq j}^{i=N} g_{ij}[n]\rho a_i[n]} = \frac{S_j}{\sigma_{\text{UE}}^2/\rho + I_j}. \quad (3)$$

Subsequently, UE j performs least squares (LS) equalization, assuming perfect knowledge of h_{jj} , by simply dividing y_j by $\sqrt{\rho}h_{jj}$ followed by Maximum Likelihood decoding to recover s_j . This would also require UE j to know the modulation scheme m_j it is receiving from BS j . Denote the symbol error probability of the recovered burst of symbols at UE j by $P_{s,j}$. The throughput $R_j[n]$ could then be approximated by¹

$$R_j[n] = W(1 - P_{s,j}[n])a_j[n] \log_2(m_j[n]), \quad (4)$$

where $P_{s,j}[n]$ is dependent on the value of $\text{SINR}_j[n]$. Note that we cannot quantify the exact dependence without knowledge of the interference statistics. Moreover, we do not consider coding (which would introduce a multiplicative coding rate term $c_j[n]$ in (4)), and only consider adaptive modulation. This is only for ease of implementation, and we compensate for this by considering both square and non-square (cross) QAM constellations to improve the granularity of $R_j[n]$, as will be highlighted in Section VI.

Let us also define the exponentially smoothed average rate $\bar{X}_j[n]$ seen by UE j as

$$\bar{X}_j[n] = (1 - 1/\tau)\bar{X}_j[n-1] + (1/\tau)R_j[n], \quad (5)$$

with $\tau > 1$ being a parameter which balances the weights of past and current transmission rates. Our objective is to maximize the long term average rate $\lim_{n \rightarrow \infty} \bar{X}_j[n]$ of each UE j by choosing the appropriate transmit decision $a_j[n]$ and modulation scheme $m_j[n] \in M$ at BS j in time slot n . In [26], this is proved to be equivalent to maximizing a utility function $U(\bar{\mathbf{X}}[n])$ for $n \rightarrow \infty$

¹We do not explicitly account for “dropped” transmissions due to large $P_{s,j}$. This can be justify based on the approach taken by hybrid ARQ (HARQ) in practical wireless systems, that accumulates the mutual information of each block even if the error rate is quite high [25].

\vec{a}_i	Transmit decision history of BS i
\vec{m}_i	Modulation history of BS i
$\vec{\mathbf{o}}_i^{\text{CON}}$	Local observation history of BS i in CON state
π_i^{CON}	Policy used to choose action a_i at BS i
r^{CON}	Single common reward distributed to all BSs
θ_i	Counter assigned to BS i
$\mathcal{E}_i^{\theta_i}$	Measured inter-BS energy vector at BS i

TABLE I: *DEC-POMDP* Notation

where

$$U(\bar{\mathbf{X}}[n]) = \sum_{j=1}^N \log(\bar{X}_j[n]), \quad (6)$$

while in [27], this is shown to be equivalent to finding the optimal rate vector $\mathbf{R}^*[n]$ in each time slot that satisfies

$$\mathbf{R}^*[n] = \arg \max_{\mathbf{R}[n]} \sum_{j=1}^N \frac{R_j[n]}{\bar{X}_j[n]}, \quad (7)$$

where $\mathbf{R}[n] = \langle R_1[n], \dots, R_N[n] \rangle$. In a given time slot n , determining $\mathbf{R}^*[n]$ is equivalent to determining $\{a_i^*[n], m_i^*[n]\} \forall i \in [N]$, which involves a combinatorial search over $(|K| + 1)^N$ possible vectors, making it computationally infeasible. Moreover, implementing a PF-based BS scheduler requires a central controller and hence is not realizable in practical decentralized BS deployments.

III. CONTENTION-BASED MEDIUM ACCESS AS A DEC-POMDP

In [20], given that a BS will only have delayed access to parameters of the UE it serves and must operate in a decentralized fashion, we formulated medium access decisions as a *decentralized partially observable Markov decision process (DEC-POMDP)* and subsequently adapted it to contention. We provide a brief overview of the aforementioned formulation in this section, with the notation adapted for adaptive modulation. Key notation has been summarized in Table I.

In each time slot n , when the counter θ_i associated with BS i expires, the BS measures the energy from each BS that is already transmitting, denoted by the vector $\mathcal{E}_i^{\theta_i} = \{\mathcal{E}_{ij}^{\theta_i}\}_{j \in [N]}$ with $\mathcal{E}_{ij}^{\theta_i}$ being the energy received at BS i from an ongoing transmission between BS j and UE j , and is given by

$$y_{ij}^{\theta_i} = \sqrt{\rho} h'_{ij} s_j a_j \mathbf{1}_{\theta_j < \theta_i} + z_{ij} \quad \mathcal{E}_{ij}^{\theta_i} = |y_{ij}^{\theta_i}|^2, \quad (8)$$

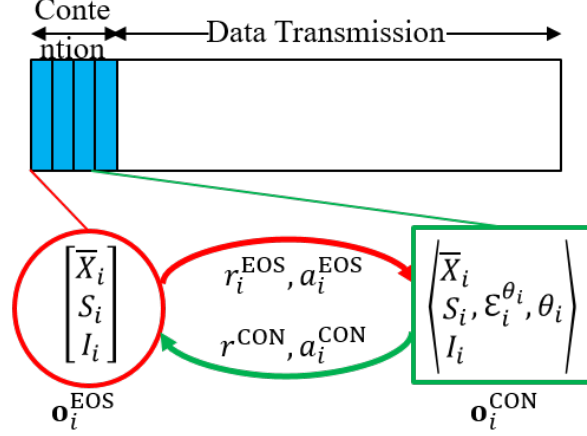


Fig. 2. The 2 state MDP at each agent capturing the actions taken and reward obtained on transitioning between the End-Of-Slot (EOS) and Contention (CON) states

where $z_{ij} \sim \mathcal{CN}(0, \sigma_{\text{BS}}^2)$, $\mathbf{1}_{\theta_j < \theta_i} = 1$ if $\theta_j < \theta_i$ and $y_{ij}^{\theta_i}$ is the received signal corresponding to $\mathcal{E}_{ij}^{\theta_i}$. We refer to the state of the BS prior to the expiration of the counter as End-Of-Slot (EOS) and post expiration of the counter as Contention (CON). As depicted in Fig. 2, in the CON state, the BS additionally has access to $\langle \mathcal{E}_i^{\theta_i}, \theta_i \rangle$. We now define the local observations $\mathbf{o}_i^{\text{EOS}}$ and $\mathbf{o}_i^{\text{CON}}$ seen by BS i in the EOS and CON states respectively.

Denote by $\mathbf{G}[n] = \{g_{ij}[n]\}$ the downlink $N \times N$ interference channel matrix in time slot n . Then the state of the system is given by $\mathbf{s}[n] \triangleq \langle \bar{\mathbf{X}}[n-1], \mathbf{G}[n] \rangle$. Each BS can only observe a relatively small part of $\mathbf{s}[n]$, depending on whether it is in the EOS or CON state. We assume that UE i feeds back its received signal power S_i and measured interference power I_i to BS i in the uplink (error-free), and that BS i keeps track of the average rate of the UE it serves, \bar{X}_i . Hence we define $\mathbf{o}_i^{\text{EOS}}$ and $\mathbf{o}_i^{\text{CON}}$ as

$$\mathbf{o}_i^{\text{EOS}}[n] = \langle \bar{X}_i[n-1], S_i[n-1], I_i[n-1] \rangle \quad \mathbf{o}_i^{\text{CON}}[n] = \langle \mathbf{o}_i^{\text{EOS}}[n], \mathcal{E}_i^{\theta_i}[n], \theta_i[n] \rangle. \quad (9)$$

Note that we do not need to explicitly notify BS i of its action-modulation scheme history $\vec{a}_i \odot \vec{m}_i$, but simply its decision to transmit or not (as contained in $S_i = g_{ii}a_i$), since \vec{m}_i is not part of $\mathbf{s}[n]$, but impacts the choice of $m_i[n]$ through $\bar{X}_i[n-1]$ which is already part of both $\mathbf{o}_i^{\text{EOS}}$ and $\mathbf{o}_i^{\text{CON}}$. We also set both r_i^{EOS} and a_i^{EOS} to 0, since these correspond to a transition within the time slot. Subsequently, $a_i^{\text{CON}} = m_i a_i$. Owing to partial observability, the policy employed to choose $m_i a_i$ in the CON state, π_i^{CON} , is defined as a mapping from the observation history $\vec{\mathbf{o}}_i^{\text{CON}}$ to $\{0, M\}$, the modulation set with the decision not to transmit added to it.

Once each BS has chosen a transmit modulation scheme, denoted by the vector $\mathbf{a} \odot \mathbf{m}[n]$, we transmit a burst of data from each BS using the chosen modulation schemes and compute $P_{s,j}$ at each UE j as described in Section II-B. Hence the transition function $T(\mathbf{s}[n], \mathbf{a} \odot \mathbf{m}[n], \mathbf{s}[n+1])$ is given by

$$\bar{X}_j[n] = \left(1 - \frac{1}{\tau}\right)\bar{X}_j[n-1] + \frac{1}{\tau}a_j[n](1 - P_{s,j}[n])\log_2(m_j[n]) \quad (10)$$

$$g_{ij}[n+1] = f(g_{ij}[n]) + n_{ij}, \quad (11)$$

where n_{ij} is the noise term, and we drop the bandwidth scaling factor W since it would just add a constant term to $U(\bar{\mathbf{X}}[L])$, where L denotes the finite time horizon of the problem. Given $\mathbf{s}[n+1]$, we can compute $\mathbf{o}_i^{\text{EOS}}[n+1] \forall i$ and each BS i will transition from $\mathbf{o}_i^{\text{CON}}[n]$ to $\mathbf{o}_i^{\text{EOS}}[n+1]$. For this transition, each BS receives a common reward $r^{\text{CON}}[n] = \sum_{j=1}^N r_j[n] \forall n > 0$ and $r^{\text{CON}}[0] = \sum_{j=1}^N \log(\bar{X}_j[0])$ where

$$r_j[n] = \log \left((1 - 1/\tau) \left(1 + \frac{R_j[n]}{(\tau - 1)\bar{X}_j[n-1]} \right) \right). \quad (12)$$

This per-timestep reward was shown in [20] to maximize $U(\bar{\mathbf{X}}[n])$ for $n \rightarrow \infty$. We will now describe distributed implementations of two single agent RL algorithms – (i) Deep Q Networks (DQN) and (ii) Proximal Policy Optimization (PPO), which are adapted to the contention-based medium access *DEC-POMDP* formulation.

IV. DEEP RL FOR MEDIUM ACCESS DEC-POMDP

A. Deep Q Networks (DQN)

In a single agent, fully-observable RL setting, an agent observes the current state $s[n]$, chooses an action $a[n]$ according to a policy π , receives a reward $r[n]$ and transitions to a new state $s[n+1]$. The objective is to learn the optimal policy π^* that maximizes the expected discounted sum of rewards $\sum_{n=0}^{\infty} \gamma^n r[n]$. Denote by $\mathcal{Q}_\pi(s[n], a)$ the expected discounted reward earned by the agent starting from state $s[n]$, taking action a , and thereafter following π . Hence the \mathcal{Q} -value corresponding to the optimal policy π^* is given as

$$\mathcal{Q}^*(s[n], a) = \max_{\pi} \mathcal{Q}_\pi(s[n], a), \quad (13)$$

which can be found by the recursive Bellman optimality equation with $n' = n + 1$ [28]

$$Q^*(s[n], a) = \mathbb{E} \left[r[n'] + \gamma \max_{a'} Q^*(s[n'], a') \mid s[n], a \right]. \quad (14)$$

In deep Q -learning, $Q_\pi(s, a)$ is represented by a neural network whose weights are optimized by minimizing $\mathbb{E}_{s,a,r,s'} [(y^{\text{DQN}} - Q(s, a))^2]$ at each iteration, with $y^{\text{DQN}} = r + \gamma \max_{a'} Q^-(s', a')$. Here $Q^-(s, a)$ denotes a target Q network that is frozen for a few iterations while updating the online network $Q(s, a)$.

B. Adapting Independent DQN to a Medium Access DEC-POMDP

To extend DQN to cooperative multi-agent settings, [29] combines DQN with independent Q -learning, such that each agent i simultaneously learns its own Q function $Q(s, a_i)$ when in state s taking action a_i and receiving a common team reward r . While Independent Q -learning can in theory lead to convergence problems due to each agent seeing a non-stationary environment, it has been surprisingly successful empirically [30], [31]. Hence we adopt the Independent DQN framework and define two Q networks at each BS i , Q_i^{EOS} and Q_i^{CON} . Using (14), we can derive the sampled Q -value updates for $\mathbf{o}_i^{\text{EOS}}$ and $\mathbf{o}_i^{\text{CON}}$ as

$$Q_i^{\text{EOS}}(\mathbf{o}_i^{\text{EOS}}) = \gamma^{\frac{1}{2}} \max_{a_i^{\text{CON}}} Q_i^{\text{CON}}(\mathbf{o}_i^{\text{CON}}, a_i^{\text{CON}}) \quad (15)$$

$$Q_i^{\text{CON}}(\mathbf{o}_i^{\text{CON}}, a_i^{\text{CON}}) = r^{\text{CON}} + \gamma^{\frac{1}{2}} Q_i^{\text{EOS}}(\mathbf{o}_i^{\text{EOS}}), \quad (16)$$

where we utilize $r_i^{\text{EOS}} = a_i^{\text{EOS}} = 0$, hence $Q_i^{\text{EOS}}(\mathbf{o}_i^{\text{EOS}}) = Q_i^{\text{EOS}}(\mathbf{o}_i^{\text{EOS}}, 0)$. By utilizing alternating Q -updates, we eliminate the need for a target Q -network as described in Section IV-A. However, unlike (14) which assumes complete state observability, Q_i^{EOS} and Q_i^{CON} only have access to local observations $\mathbf{o}_i^{\text{EOS}}$ and $\mathbf{o}_i^{\text{CON}}$ and also are not aware of $\mathbf{a} \odot \mathbf{m} - \{a_i^{\text{CON}}\}$. We describe the features of our approach designed to provide for this partial observability in Section IV-E and IV-F.

C. Proximal Policy Optimization (PPO)

Given a state s and an action a , we have three terms associated with a typical single agent RL problem: $\pi(a|s; \Theta)$, $Q^\pi(s, a)$ and $V^\pi(s)$. We denote by $\pi(a|s; \Theta)$ a policy parameterized by Θ that returns the probability of an agent selecting action a in state s . If an agent starts from state s , chooses action a and thereafter follows π , the expected reward accumulated is represented

by $\mathcal{Q}^\pi(s, a)$. Finally, $V^\pi(s)$ denotes the expected reward accumulated by an agent following π starting from state s . Policy-based model-free methods directly parameterize the policy $\pi(a|s; \Theta)$ and update Θ by performing gradient ascent on $J(\Theta) = \mathbb{E}[\gamma^n r[n]]$. The gradient is given by $\nabla_\Theta \log \pi(a|s; \Theta) \mathcal{Q}^\pi(a|s)$. To reduce the variance of this unbiased estimate of $\nabla_\Theta J(\Theta)$, a learnt baseline $b(s) \approx V^\pi(s)$ is subtracted [32] such that

$$\nabla_\Theta J(\Theta) = \nabla_\Theta \log \pi(a|s; \Theta) (\mathcal{Q}^\pi(a|s) - V^\pi(s)), \quad (17)$$

where $A(s, a) = \mathcal{Q}^\pi(a|s) - V^\pi(s)$ is known as the *advantage*. This approach can then be viewed as an actor-critic architecture, where actor refers to $\pi(a|s)$ while $V^\pi(s)$ is the critic. In actor-critic algorithms, both the actor and critic are represented by two separate neural networks, $\pi(a|s; \Theta)$ and $V(s; \vartheta)$, parameterized by Θ and ϑ respectively, and the following loss function is minimized

$$L(\Theta, \vartheta) = -J(\Theta) + (V(s, \vartheta) - V^{\text{target}}(s))^2. \quad (18)$$

A truncated version of generalized advantage estimation (GAE) [33] is traditionally utilized to compute $V^{\text{target}}(s_t)$ as

$$V(s_t; \vartheta) + \delta_t + (\gamma\lambda)\delta_{t+1} + \dots + (\gamma\lambda)^{T-t+1}\delta_{T-1}, \quad (19)$$

$$\text{where } \delta_t = r_t + \gamma V(s_{t+1}; \vartheta) - V(s_t; \vartheta). \quad (20)$$

Proximal Policy Optimization (PPO) [23] alters the loss function in (18) in two ways. First, it replaces $J(\Theta) = \mathbb{E}[\pi(a|s; \Theta)A(s, a)]$ with

$$L^{\text{CLIP}}(\Theta) = \mathbb{E}[\min(r(\Theta)A, \text{clip}(r, 1 - \epsilon, 1 + \epsilon)A)], \quad (21)$$

$$\text{where } r(\Theta) = \pi(a|s; \Theta) / \pi(a|s; \Theta_{\text{old}}). \quad (22)$$

The clip term in $L^{\text{CLIP}}(\Theta)$ removes the incentive for moving r outside of the interval $[1 - \epsilon, 1 + \epsilon]$. The minimum of the clipped and unclipped objective is then taken so that the final objective is a lower bound on the unclipped objective. Hence, the motivation for this modified metric is to not reward excessively large policy updates, while the ‘‘surrogate objective’’ $r(\Theta)A$ arises from a policy gradient approach known as trust region policy optimization (TRPO) [34], a precursor to PPO. The term $\pi(a|s; \Theta_{\text{old}})$ in (22) is a constant that corresponds to the evaluation of the policy π at the given (s, a) using the current weights Θ_{old} of the policy NN. Secondly, PPO

adds an entropy bonus $S[\pi(\cdot|s; \Theta)]$ to ensure sufficient exploration. Consequently, the final PPO objective $L^{\text{PPO}}(\Theta, \vartheta)$ which is maximized each iteration is given by [23]

$$L^{\text{PPO}}(\Theta, \vartheta) = L^{\text{CLIP}}(\Theta) - c_1(V(s, \vartheta) - V^{\text{target}}(s))^2 + c_2 S[\pi(\cdot|s; \Theta)]. \quad (23)$$

D. Adapting PPO to a Medium Access DEC-POMDP

We now define N loss functions $L(\Theta_i^{\pi^{\text{CON}}}, \vartheta_i^{V^{\text{CON}}}, \vartheta_i^{V^{\text{EOS}}})$ corresponding to each BS i , by adapting (23) to the 2-state MDP presented in Fig. 2, as

$$L_{\text{EOS-CON}}^{\text{PPO}}(\Theta_i^{\pi^{\text{CON}}}, \vartheta_i^{V^{\text{CON}}}, \vartheta_i^{V^{\text{EOS}}}) = L^{\text{PPO}}(\Theta_i^{\pi^{\text{CON}}}, \vartheta_i^{V^{\text{CON}}}) - c_3 L^{\text{VF}}(\vartheta_i^{V^{\text{EOS}}}), \quad (24)$$

at each BS i , where

$$L^{\text{VF}}(\vartheta_i^{V^{\text{EOS}}}) = (V_i^{\text{EOS}}(\mathbf{o}_i^{\text{EOS}}) - V_i^{\text{target, EOS}}(\mathbf{o}_i^{\text{EOS}}))^2, \quad (25)$$

while a similar expression for $L^{\text{VF}}(\vartheta_i^{V^{\text{CON}}})$ is already part of $L^{\text{PPO}}(\Theta_i^{\pi^{\text{CON}}}, \vartheta_i^{V^{\text{CON}}})$. Note that the only key changes from (23) are that we have added a term for training V_i^{EOS} and the input to the EOS and CON NNs will be $\mathbf{o}_i^{\text{EOS}}$ and $\mathbf{o}_i^{\text{CON}}$ respectively, instead of the full system state s . To overcome this partial observability, an LSTM layer is introduced in V_i^{CON} , V_i^{EOS} and π_i^{CON} at every BS i as will be explained in Section IV-E. Now, to compute $V_i^{\text{target, CON}}$ and $V_i^{\text{target, EOS}}$, we first observe that (20), when applied to the EOS-CON transition yields

$$\delta_{i,n}^{\text{CON}} = r[n] + \gamma^{\frac{1}{2}} V_i^{\text{EOS}}(\mathbf{o}_i^{\text{EOS}}[n+1]) - V_i^{\text{CON}}(\mathbf{o}_i^{\text{CON}}[n]) \quad (26)$$

$$\delta_{i,n}^{\text{EOS}} = \gamma^{\frac{1}{2}} V_i^{\text{CON}}(\mathbf{o}_i^{\text{CON}}[n]) - V_i^{\text{EOS}}(\mathbf{o}_i^{\text{EOS}}[n]). \quad (27)$$

Note that the factor of $\gamma^{\frac{1}{2}}$ in (26) and (27) is simply meant to keep the overall discount factor to γ in one time step. Substituting (26) and (27) into (19) and replacing T by the episode length L , we obtain

$$V_i^{\text{target, EOS}} = V_i^{\text{EOS}}(\mathbf{o}_i^{\text{EOS}}) + \delta_{i,n}^{\text{EOS}} + (\gamma^{\frac{1}{2}} \lambda) \delta_{i,n}^{\text{CON}} + \dots + (\gamma^{\frac{1}{2}} \lambda)^{L-n+1} \delta_{i,L-1}^{\text{EOS}} \quad (28)$$

$$V_i^{\text{target, CON}} = V_i^{\text{CON}}(\mathbf{o}_i^{\text{CON}}) + \delta_{i,n}^{\text{CON}} + (\gamma^{\frac{1}{2}} \lambda) \delta_{i,n+1}^{\text{EOS}} + \dots + (\gamma^{\frac{1}{2}} \lambda)^{L-n+1} \delta_{i,L-1}^{\text{CON}} \quad (29)$$

$$\hat{A}_i^{\text{CON}} = V_i^{\text{target, CON}}(\mathbf{o}_i^{\text{CON}}) - V_i^{\text{CON}}(\mathbf{o}_i^{\text{CON}}). \quad (30)$$

\hat{A}_i^{CON} provides an estimate of A_i^{CON} , which will be utilized for computing $L^{\text{CLIP}}(\Theta_i^{\pi^{\text{CON}}})$ by substituting it in place of A in (21).

E. Deep Recurrent Learning

The adaptations of Independent DQN and PPO to a Medium Access DEC-POMDP presented in Section IV-B and IV-D respectively would not hold if the observations $\mathbf{o}_i^{\text{EOS}}$ and $\mathbf{o}_i^{\text{CON}}$ were simply provided as input to the neural networks. Two modifications are required, and we describe the first - adding recurrency - in this section. In [35], they show that adding an LSTM layer [36] in a Q -network helps to learn the correct Q -values from sequences of observations in a POMDP setting, where the agent only has access to a partial observation of the state.

We incorporate a LSTM layer into each of the neural networks - Q_i^{CON} , Q_i^{EOS} , V_i^{CON} , π_i^{CON} and V_i^{EOS} . An example of such a neural architecture is shown in Fig. 6. π_i^{CON} receives as input the hidden and cell state, $state_h_{i,n-1}$ and $state_c_{i,n-1}$ respectively in time slot n , and updates them to $state_h_{i,n}$ and $state_c_{i,n}$. The hidden and cell state at BS i act as compressed representations of the observation history $\vec{\mathbf{o}}_i^{\text{CON}}$.

However, we are attempting to solve a *DEC-POMDP*, not simply a POMDP, hence simply adding recurrency will not suffice. One inherent feature of the design of observation $\mathbf{o}_i^{\text{CON}}$ is the energy vector $\mathcal{E}_i^{\theta_i}$ that provides the BS i with knowledge of all $a_j = 1$ for $\{j : \theta_j < \theta_i\}$. The other feature we incorporate aims at providing a greater degree of centralization during training, and is described next.

F. Decentralized Actor Centralized Critic

Naive policy gradient methods perform poorly even in simple multi-agent settings [37]. For instance, in the current setting, via recurrent neural networks, BS i selects an action a_i^{CON} based on the policy $\pi_i^{\text{CON}} : \langle \vec{\mathbf{o}}_i, \vec{\mathcal{E}}_i^{\theta_i}, \vec{\theta}_i \rangle \rightarrow \{0, M\}$. However, as is evident from the PF scheduler (7), a_i^{CON} can be correctly determined only if \bar{X}_j and $a_j \forall j \neq i$ are known along with the interference channel matrix \mathbf{G} . Hence the learned policy conditioned only on $\langle \vec{\mathbf{o}}_i, \vec{\mathcal{E}}_i^{\theta_i}, \vec{\theta}_i \rangle$ will exhibit high variability, increasing the variance of the gradients. Consequently, to stabilize the training and improve the learnt policy, we incorporate a *decentralized actor centralized critic* approach, first proposed in [37].

First we note that only π_i^{CON} is required for generating an episode i.e. at test time, while the remaining NNs are employed only during training. Hence, we can use centralized information for

training, provided the input to π_i^{CON} remains $\mathbf{o}_i^{\text{CON}}$. We can train the *critics* centrally to overcome the challenge of a non-stationary non-Markov environment, while executing the policies learnt by the *actors* distributedly. To this effect, we change the input to V_i^{EOS} , Q_i^{EOS} and V_i^{CON} by replacing $\mathbf{o}_i^{\text{EOS}}$ with \mathbf{s}^{EOS} at each BS i . While we defined $\mathbf{o}_i^{\text{EOS}}[n+1] = \langle \bar{X}_i[n], S_i[n], I_i[n] \rangle$, we have $\mathbf{s}^{\text{EOS}}[n+1] = \langle \bar{\mathbf{X}}[n], \mathbf{S}[n], \mathbf{I}[n] \rangle$ i.e. it will contain the average rate, signal and interference power of all UEs in the previous time slot. Hence the input to V_i^{CON} will be $\langle \mathbf{s}^{\text{EOS}}, \mathcal{E}_i^{\theta_i}, \theta_i \rangle$, while the input to π_i^{CON} and Q_i^{CON} remains unchanged.

G. Generating an Episode

An episode denotes a collection of L consecutive time slots. At the beginning of time slot, BS i draws a random counter θ_i as shown in the table on the left in Fig. 3. When this counter expires, BS i transitions from EOS to CON, and chooses an action $a_i^{\text{CON}} = a_i m_i$. Denote by $M' = \{0, M\}$. The example shown in Fig. 3 depicts the PPO-based approach, for which

$$a_i m_i = \max_{k \in [K+1]} M' [\pi_i^{\text{CON}}(\mathbf{o}_i^{\text{CON}})[k]], \quad (31)$$

while for the DQN-based approach,

$$a_i m_i = \max_{k \in [K+1]} M' [Q_i^{\text{CON}}(\mathbf{o}_i^{\text{CON}}, k)]. \quad (32)$$

Note that while generating an episode during the training of the algorithm, we simply sample the action randomly from the probability distribution outputted by $\pi_i^{\text{CON}}(\mathbf{o}_i^{\text{CON}})$ for PPO, or use an ϵ -greedy policy to choose the action to provide for the exploration-exploitation trade-off [12] for DQNs. This is collectively denoted by the ‘‘Action Select’’ box in Fig. 3.

In the $N = 2$ example shown in Fig 3, once BS 1 has chosen to transmit ($a_1 = 1$) and chosen a modulation scheme $m_1 = 4$, BS 0 is informed of $a_1 = 1$ through a non-zero $\mathcal{E}_{01}^{\theta_0}$ input to both π_0^{CON} and V_0^{CON} . However, if BS 1 had chosen not to transmit, BS 0 would not be aware if the $\mathcal{E}_{01}^{\theta_0}$ term is 0 because θ_1 has not expired or BS 1 has set $a_1 = 0$. Once all the BSs have chosen a transmit modulation scheme $\mathbf{a} \odot \mathbf{m} = \{a_0 m_0, a_1 m_1\}$, we compute $P_{s,j}$ at each UE j and update the rates to $\bar{\mathbf{X}}[n]$ as described in Section II-B. These determine the observations $\mathbf{o}_i^{\text{EOS}}$ for the next time slot. In the next time slot $n + 1$, a new counter θ'_i is drawn at each BS i and the process repeated. Note that the counters are unique in the example shown only for simplicity, and the simulations do allow for counter collisions.

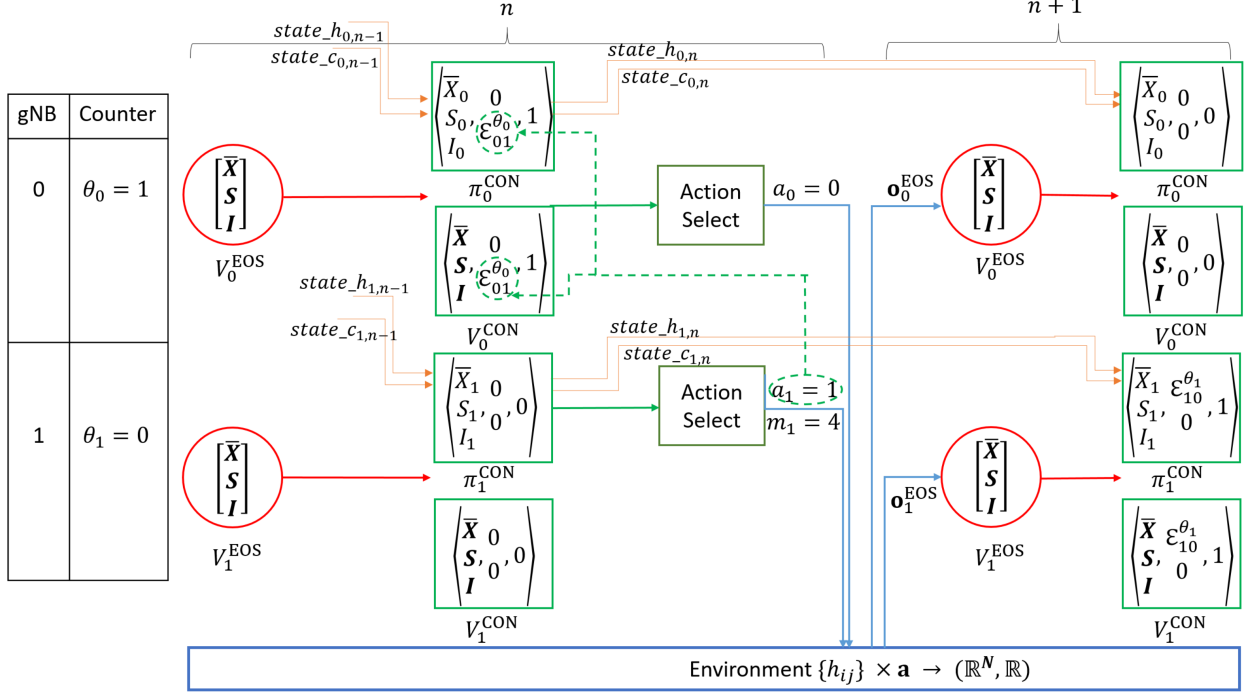


Fig. 3. Information flow between BSs and the environment. The evolution of the hidden and cell state, $state_{h_{i,n}}$ and $state_{c_{i,n}}$ is shown only for π_i^{CON} , but holds for V_i^{EOS} and V_i^{CON} too. The red outline denotes EOS NNs and the green outline, the CON NNs.

V. SIMULATION DETAILS

The performance metric is the expected cumulative reward $\sum_{n=0}^L \gamma^n r^{\text{CON}}[n]$ introduced in Section III, with $r[n]$ given by (12). A smoothing window of $\tau = 10$, discount factor $\gamma = 1 - 10^{-6}$ and $L = 2000$ time slots are used in all the subsequent simulations. We set $\gamma \rightarrow 1$ so that $\sum_n \gamma^n r^{\text{CON}}[n] \rightarrow U(\bar{\mathbf{X}}[n])$. With a typical UE velocity of 3 km/h in a pedestrian setting, $L = 2000$ time slots corresponds to $\sim 2\text{s}$ - a duration for which it is reasonable to consider the UE to be stationary.

A. Data Generation

We consider two deployment scenarios - an indoor and an outdoor layout. The indoor hotspot deployment is intended to capture typical indoor situations such as office environments comprised of open cubicle areas, walled offices, open areas and corridors (InH-Office). The baseline layout is shown in Fig. 4a. The BS's are mounted at a height of 3m on the ceiling. 120 UEs are uniformly distributed in a 120m x 50m layout and have a height of 1.5m. Each BS is associated with 10 UEs. The pathloss (PL) model between nodes (BS and UEs) captures Line-Of-Sight(LOS)/ Non-

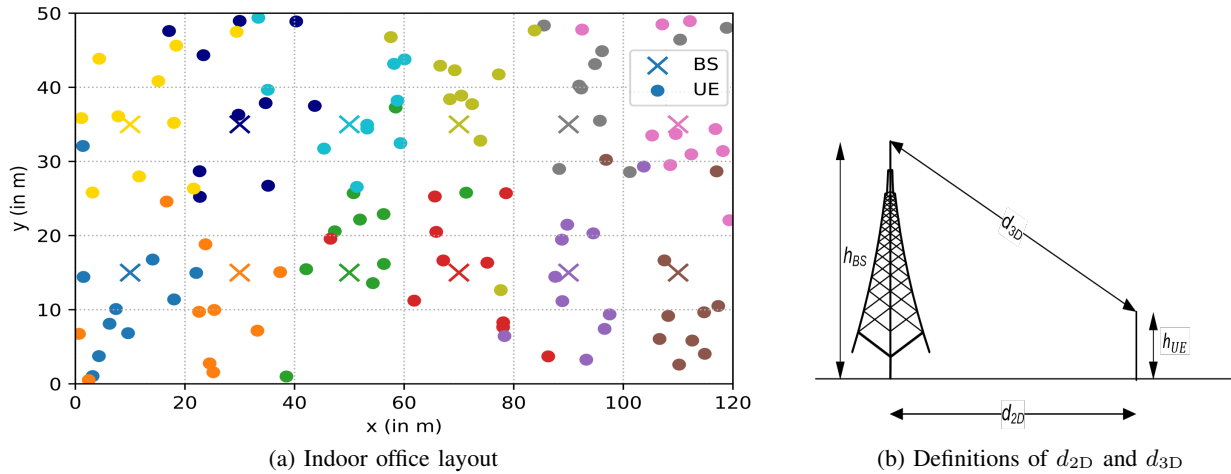


Fig. 4. InH-Office layout used for simulations.

LOS/NLOS	Pathloss [dB], f_c is in GHz and d is in meters	Shadow fading std [dB]	Applicability range
LOS	$PL_{LOS} = 32.4 + 17.3 \log_{10}(d_{3D}) + 20 \log_{10}(f_c)$	$\sigma_{SF} = 3$	$1\text{m} \leq d_{3D} \leq 150\text{m}$
NLOS	$PL_{NLOS} = \max(PL_{LOS}, PL'_{NLOS})$ $PL'_{NLOS} = 17.3 + 38.3 \log_{10}(d_{3D}) + 24.9 \log_{10}(f_c)$	$\sigma_{SF} = 8.03$	$1\text{m} \leq d_{3D} \leq 150\text{m}$

TABLE II: 3GPP InH-Office PL Model. Shadow fading distribution is log-normal. Reproduced from [38].

Line-Of-Sight(NLOS) properties of a link, frequency dependent path loss for LOS/ NLOS links and shadowing as part of large-scale fading parameters, and is given in Table II. In accordance with the indoor - open office model [38], the links are designated as LOS/ NLOS probabilistically with Pr_{LOS} given by

$$\text{Pr}_{\text{LOS}} = \begin{cases} 1 & , d_{2D} \leq 5\text{m} \\ \exp\left(-\frac{d_{2D}-5}{70.8}\right) & , 5\text{m} < d_{2D} \leq 49\text{m} \\ 0.54 \exp\left(-\frac{d_{2D}-49}{211.7}\right) & , 49\text{m} < d_{2D} \end{cases} \quad (33)$$

The outdoor layout is an Urban Micro (UMi) layout [38], where the BSs are mounted below rooftop levels of surrounding buildings. This layout is intended to capture real-life outdoor scenarios such as a city square. The baseline layout is shown in Fig. 5. There are 19 BSs distributed in a hexagonal layout with an inter-BS separation of 200m. Each BS is at a height

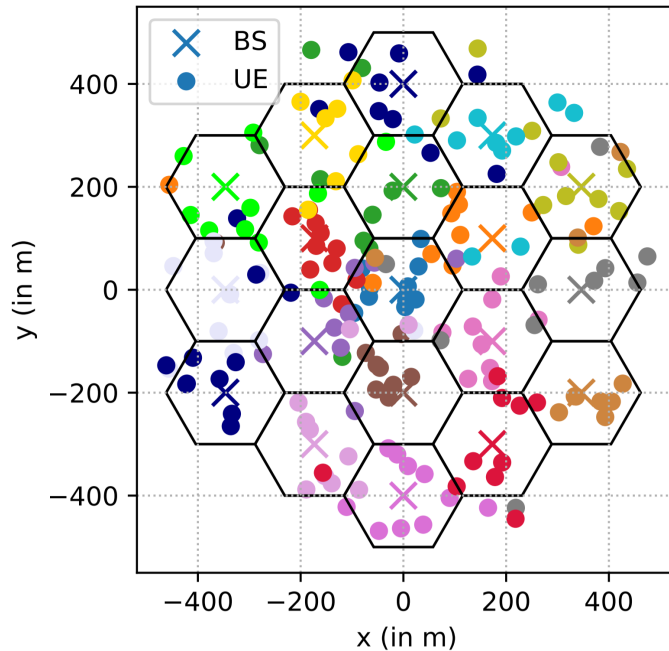


Fig. 5. 3GPP UMi-Street Canyon layout used for simulations.

of 10m, and 190 UEs are uniformly distributed in the hexagonal layout shown, each BS being associated with 10 UEs. From these, 20% of the UEs are outdoor and at a height of 1.5 m, while the height of the remaining indoor UEs (in m) is given by

$$h_{\text{UE}} = 3(n_{fl} - 1) + 1.5 \quad (34)$$

$$n_{fl} \sim \text{uniform}(1, N_{fl}) \quad \text{where } N_{fl} \sim \text{uniform}(4, 8) \quad (35)$$

The UMi PL model has properties similar to the InH-Office model and is given in Table III. The links for the UMi- Street Canyon model are also designated as LOS/ NLOS probabilistically with Pr_{LOS} given by

$$\text{Pr}_{\text{LOS}} = \begin{cases} 1 & , d_{2\text{D-out}} \leq 18\text{m} \\ \frac{18}{d_{2\text{D-out}}} + \exp\left(-\frac{d_{2\text{D-out}}}{36}\right) \left(1 - \frac{18}{d_{2\text{D-out}}}\right) & , 18\text{m} < d_{2\text{D-out}} \end{cases} \quad (36)$$

where $d_{2\text{D-out}} = d_{2\text{D}} - d_{2\text{D-in}}$ with $d_{2\text{D-in}} = \min(\text{uniform}(0, 25), \text{uniform}(0, 25))\text{m}$ for indoor UEs and $d_{2\text{D-in}} = 0$ for outdoor UEs. The center frequency f_c used for modeling is 6 GHz.

The temporal evolution of the channel coefficients h_{ij} and h'_{ij} is modelled as a slow fading channel using a first order IID filter. With the large scale fading coefficient (from the PL model)

LOS/NLOS	Pathloss [dB], f_c is in GHz and d is in meters	Shadow fading std [dB]	Applicability range
LOS	$PL_{LOS} = \begin{cases} PL_1 & 10m \leq d_{2D} \leq d'_{BP} \\ PL_2 & d'_{BP} \leq d_{2D} \leq 5km \end{cases}$ $PL_1 = 32.4 + 21 \log_{10}(d_{3D}) + 20 \log_{10}(f_c)$ $PL_2 = 32.4 + 40 \log_{10}(d_{3D}) + 20 \log_{10}(f_c) - 9.5 \log_{10}((d'_{BP})^2 + (h_{BS} - h_{UE})^2)$	$\sigma_{SF} = 4$	$1.5m \leq h_{UE} \leq 22.5m$ $h_{BS} = 10m$
NLOS	$PL_{NLOS} = \max(PL_{LOS}, PL'_{NLOS})$ <p style="text-align: center;">for $10m \leq d_{2D} \leq 5km$</p> $PL'_{NLOS} = 22.4 + 35.3 \log_{10}(d_{3D}) + 21.3 \log_{10}(f_c) - 0.3(h_{UE} - 1.5)$	$\sigma_{SF} = 7.82$	$1.5m \leq h_{UE} \leq 22.5m$ $h_{BS} = 10m$

TABLE III: 3GPP UMi-Street Canyon PL Model. Shadow fading distribution is log-normal. Breakpoint distance $d'_{BP} = 4h'_{BS}h'_{UE}f_c/c$ where h'_{BS} and h'_{UE} are the effective BS and UE antenna heights given by $h'_{BS} = h_{BS} - 1$ and $h'_{UE} = h_{UE} - 1$. Reproduced from [38].

denoted by $g_{ls} = g_0$, and the small scale fading coefficient by h_{ss} , we have

$$h_{ss}[n] = (1 - \alpha)h_{ss}[n - 1] + \alpha z[n] \quad g[n] = g_0 |h_{ss}[n]|^2, \quad (37)$$

with $h_{ss}[0] = 1$, $z[n] \sim \mathcal{CN}(0, \sigma_{ss}^2)$ and $\sigma_{ss}^2 = (1 - (1 - \alpha)^2)/\alpha^2$. The length of one slot T ranges from 1 to 9 ms [5]. Solving $0.5 = (1 - \alpha)^n$ with $\alpha = 0.1$ yields $n = 7$. Hence, the time taken for the channel to decorrelate 50% = $7T$, which is on the order of 10 ms, typical for a pedestrian setting. Key parameters used for generating the data are summarized in Table IVa.

We set $M = \{4, 8, 16, 32, 64, 128, 256\}$. For (i) M-PSK constellation $M_k = \{8\}$, its symbol s is given by

$$\exp(2\pi j\beta/M_k), \quad \beta = 0, \dots, M_k - 1 \quad (38)$$

(ii) for square constellations $M_k \in \{4, 16, 64, 256\}$, the in-phase and quadrature components of its symbol s independently takes values in the set

$$\left\{ \sqrt{\frac{3}{2(M_k - 1)}} (2\beta + 1 - \sqrt{M_k}) \right\}, \quad \beta = 0, \dots, \sqrt{M_k} - 1 \quad (39)$$

(iii) and for cross QAM constellations $M_k \in \{32, 128\}$, we define a block parameter $v = \sqrt{\frac{M}{32}}$ [21]. Cross-QAM constellation can then be constructed by a square block array with the 4 corner blocks deleted, each block with v^2 uniform distributed points [39]. For all constellations, we ensure that the constellation points are normalized to unit power in expectation.

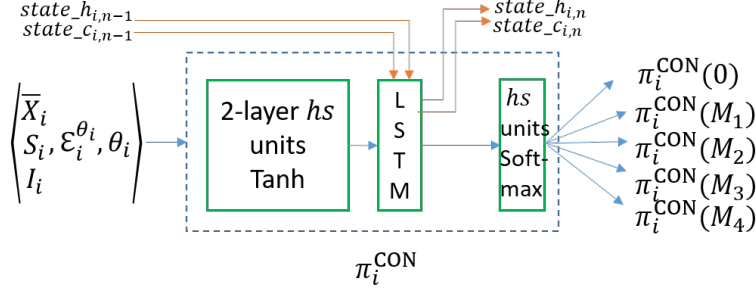


Fig. 6. NN architecture of π_i^{CON} with $K = 4$. 0 corresponds to not transmitting, while M_1 to M_4 correspond to the modulation schemes to choose from.

B. NN Architectures

Both π_i^{CON} and Q_i^{CON} have $K + 1$ output arms, corresponding to the choice of K modulation schemes when $a_i = 1$, and $a_i = 0$. Q_i^{EOS} always has a default action of $a^{\text{EOS}} = 0$, hence Q -value of $a^{\text{EOS}} = 1$ is discarded. Finally, V_i^{CON} and V_i^{EOS} have an output size of 1. The architectures of all NNs involved is identical with the exception of input and output size, with the input size being determined by whether the input is $\mathbf{o}_i^{\text{EOS}}$, $\mathbf{o}_i^{\text{CON}}$ or \mathbf{s}^{EOS} . The architecture for π_i^{CON} is shown in Fig. 6. Since a π network is depicted, the last layer has a Softmax activation so that probabilities of the respective actions are outputted. For Q_i^{CON} , we drop the Softmax activation and output $\{A_i^{\text{CON}}(0), \dots, A_i^{\text{CON}}(M_K)\}$ and V_i^{CON} . We then utilize dueling [40] to compute the Q_i^{CON} -values.

C. PPO and DQN Training Procedure

A policy gradient approach differs from a DQN-based approach in that due to its increased speed of convergence, the batch of episodes used in every iteration have to be generated using the most recent weights Θ^{CON} , ϑ^{CON} and ϑ^{EOS} , unlike the replay memories maintained while training the DQNs in [20]. Hence, in each iteration, N_{batch} episodes are generated by N_{batch} π_i^{CON} (actors) at each BS i acting in parallel.

In order to have a fair comparison with the DQN algorithm from [20], we make two changes in the implementation of distributed DQN from [20]. Firstly, we alter the input to Q_i^{EOS} to \mathbf{s}^{EOS} in place of $\mathbf{o}_i^{\text{EOS}}$ as explained in IV-F. Secondly, in each iteration, N_{batch} episodes are generated using the current Q_i^{EOS} and Q_i^{CON} , in place of the replay memories D^{EOS} and D^{CON} utilized in [20] that added one episode generated using the current NNs and removed the oldest episode every iteration. The methodology for both the PPO and DQN based medium access algorithms

used in this paper have been presented as Algorithm 1 and 2 respectively. Parameters used for training the NNs are summarized in Table Vb.

Algorithm 1: Spectrum Sharing Proximal Policy Optimization

```

for iteration = 1, 2, ... do
  for actor = 1, 2, ...,  $N_{\text{batch}}$  do
    Generate an episode of  $L$  time slots as detailed in Section IV-G.
    In each time slot, each BS  $i$  chooses not to transmit / transmit with modulation
    scheme  $M_k$  with probability  $\pi_i^{\text{CON}}[0]$  /  $\pi_i^{\text{CON}}[k]$ .
  end
  for  $i = 1, 2, \dots, N$  do
    Compute target values  $V_i^{\text{target, EOS}}, V_i^{\text{target, CON}}$  and advantage estimate  $\hat{A}_i^{\text{CON}}$  using
    (28), (29) and (30) respectively at each time for all actors in parallel.
    By performing gradient ascent on  $L_{\text{EOS-CON}}^{\text{PPO}}(\Theta_i^{\pi^{\text{CON}}}, \vartheta_i^{V^{\text{CON}}}, \vartheta_i^{V^{\text{EOS}}})$ , update
    weights of  $\pi_i^{\text{CON}}, V_i^{\text{CON}}$  and  $V_i^{\text{EOS}}$ . Perform 1 epoch with batch size  $N_{\text{batch}} \times L$ 
  end
end

```

Algorithm 2: Spectrum Sharing Deep Q Learning

```

for iteration = 1, 2, ... do
  for actor = 1, 2, ...,  $N_{\text{batch}}$  do
    Generate an episode of  $L$  time slots as detailed in Section IV-G.
    In each time slot, each BS  $i$  chooses a transmit modulation scheme from
     $M' = \{0, M\}$  randomly w.p.  $\epsilon$  or greedily based on  $Q_i^{\text{CON}}$  w.p.  $1 - \epsilon$ .
  end
  for  $i = 1, 2, \dots, N$  do
    Compute labels  $\mathcal{L}_i^{\text{EOS}}(\mathbf{s}^{\text{EOS}}) = \gamma \max_{a_i^{\text{CON}}} Q_i^{\text{CON}}(\mathbf{o}_i^{\text{CON}}, a_i^{\text{CON}})$  and
     $\mathcal{L}_i^{\text{CON}}(\mathbf{o}_i^{\text{CON}}, a_i^{\text{CON}}) = r_i^{\text{CON}} + \gamma Q_i^{\text{EOS}}(\mathbf{s}^{\text{EOS}})$  at each time for all actors in parallel.
    Perform 1 epoch of gradient descent with batch size  $N_{\text{batch}} \times L$  on MSE loss to
    update weights of  $Q_i^{\text{EOS}}$  and  $Q_i^{\text{CON}}$ .
  end
end

```

D. PF Scheduler and ED Threshold Baselines

Three baselines are used for benchmarking the performance of the RL PPO and DQN algorithms - centralized PF, genie-based adaptive ED and a single ED threshold of $E_0 = -72$ dBm. The centralized PF-based BS scheduler was presented in Section II-B, and we utilize it to determine whether a BS will transmit in each time slot, by setting $R_j[n] = W \log_2(1 + \text{SINR}_j[n])$. The single ED threshold baseline allows a BS to transmit if the received sum of energies of the

N	InH: 12 UMi: 19	Initial Learning Rate	$\eta : 5 \times 10^{-5}$
Transmit Power ρ	InH: 23 dBm UMi: 44 dBm	Learning Rate Decay	0.85 / 20 updates
Noise PSD	-174 dBm/Hz	Weight Decay	0.001
Bandwidth	20 MHz	Optimizer	Adam [41]
UE Noise Figure	9 dB	ϵ, γ, L	0.2, 1 - 1e-6, 2000
BS Noise Figure	5 dB	GAE coefficient λ	0.95
Fading Coefficient α	0.1	c_1, c_2, c_3	1, 0.01, 1
		$ state_h_{i,n} $ for (PPO, DQN)	(128, 256)
		h_s for (PPO,DQN)	(256,512)

(a) Data Generation Parameters

(b) RL Training Parameters

TABLE IV: Simulation Parameters

already transmitting BSs is less than E_0 i.e. BS i transmits if $\sum_{j=1}^N \mathcal{E}_{ij}^{\theta_i} < E_0$. The ‘‘Adaptive ED’’ is a configuration adaptive ED threshold, which finds the ED threshold that maximizes $\sum_{n=0}^L \gamma^n r[n]$ for the given configuration of UEs from a set of ED thresholds ranging from -22 dBm to -92 dBm. Using both these baselines as well, each BS i decides whether or not to transmit in the given time slot, which is denoted by a_i .

Suppose BS i has chosen to transmit. Then to determine which modulation scheme m_i is chosen by BS i , we solve the following

$$m_i = \arg \max_j \|(1 - P_{s,j}) \log_2 M_j\|_2^2 \quad (40)$$

where $P_{s,j}$ is approximated by [42] as

$$P_{s,j} = \begin{cases} 1 - \left(1 - \frac{2(\sqrt{M_j}-1)}{\sqrt{M_j}} Q\left(\sqrt{\frac{3 \cdot \text{SINR}_i}{M_j-1}}\right)\right)^2 & M_j = \{4, 16, 64, 256\}, \\ 2Q\left(\sqrt{2 \cdot \text{SINR}_i \sin^2\left(\frac{\pi}{M_j}\right)}\right) & M_j = 8, \\ 4Q\left(\sqrt{\frac{3 \cdot \text{SINR}_i}{M_j-1}}\right) & M_j = \{32, 128\}. \end{cases} \quad (41)$$

Note that the approximations for non-square constellations in (41) are upper bounds, hence we utilize $\max\{P_{s,j}, 1\}$ for $M_j = \{8, 32, 128\}$. Having determined $a_i m_i$ at each BS, we recompute $P_{s,i}$ via simulation as described in Section II-B, and subsequently compute the UE throughputs. There are two key observations that can be made here - first, by utilizing (40) to compute m_i , we are assuming a genie in all baselines that can provide BS i with the value of SINR_i , once each BS has decided whether or not to transmit. No such genie is required by the RL algorithms. Second, if we were simply determining whether or not to transmit, then centralized

PF would be an upper bound on the attainable reward [27]. However, with $K + 1$ actions to choose from per BS, finding the modulation schemes that would maximize the PF metric would require $(K + 1)^N$ simulations that compute $P_{s,j} \forall j$ per time slot which is not feasible. Hence, we continue to choose a binary decision a_i from 2^N options for the PF scheduler at BS i , and then compute the modulation scheme m_i using (40) and (41).

VI. RESULTS AND DISCUSSION

To highlight the scalability and generalizability of the proposed RL approach, we present results on both the 12 BS indoor InH-Office layout and the 19 BS outdoor UMi-Street Canyon layout from [38]. Henceforth, we will refer to the position of the BSs as a *Layout*, and the position of the UEs as a configuration. Since we have 1 UE scheduled per BS and 10 UEs associated with each BS, we have 10^{12} and 10^{19} possible configurations for the two layouts respectively. For both of the layouts, we randomly sample 2×10^4 configurations. From these, we randomly sample $N_{\text{batch}} = 8$ configurations and generate one episode using each of the N_{batch} configurations at each training iteration.

The validation curve is shown for the InH-Office and UMi-Street Canyon layouts in Fig. 7a and 8a respectively, along with the PF, ED = -72 dBm and Adaptive ED baselines. It is obtained by evaluating the trained models obtained after every 10 iterations on 10 randomly sampled configurations (not part of the training set) and averaged over 10 realizations of each configuration. For every realization of each UE configuration, we compute the sum rate $W \sum_{j=1}^N \bar{X}_j[L]$ and max rate $W \max_j \bar{X}_j[L]$ obtained using the RL PPO and DQN algorithms at the end of L time-steps. The sum and max rate, averaged over all realizations and configurations, and evaluated using the trained model obtained after every 10 iterations, are plotted for InH-Office and UMi-Street Canyon layouts in Fig. 7b and 8b respectively, along with the corresponding PF and Adaptive ED baselines. Note that for both the UMi-Street Canyon results in Fig. 8, the PF baseline has not been plotted since it is not computationally feasible to evaluate 2^{19} transmit decisions in each time slot.

RL significantly outperforms Adaptive ED: In both layouts, the reward accumulated by the RL algorithms is significantly higher than even the genie-aided adaptive ED baseline as seen in Fig 7a and 8a. This gain is also reflected in the significant increase in sum rate in Fig. 7b and 8b. At the same time, we can see that ED = -72dBm provides significantly varying degree of fairness in different scenarios, depending on the BS separation.

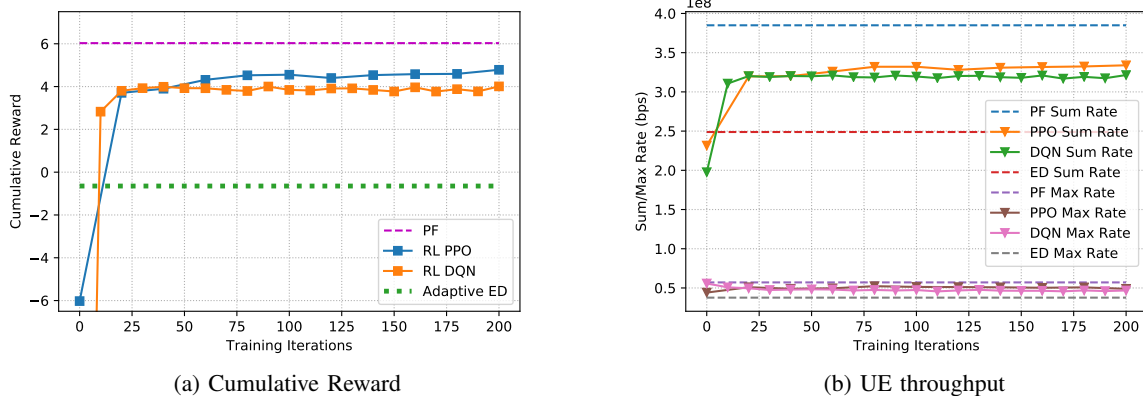


Fig. 7. Results evaluated on Validation Set for InH-Office layout. For *Layout 1*, ED = -72 dBm has a reward of -22.03 and has not been shown.

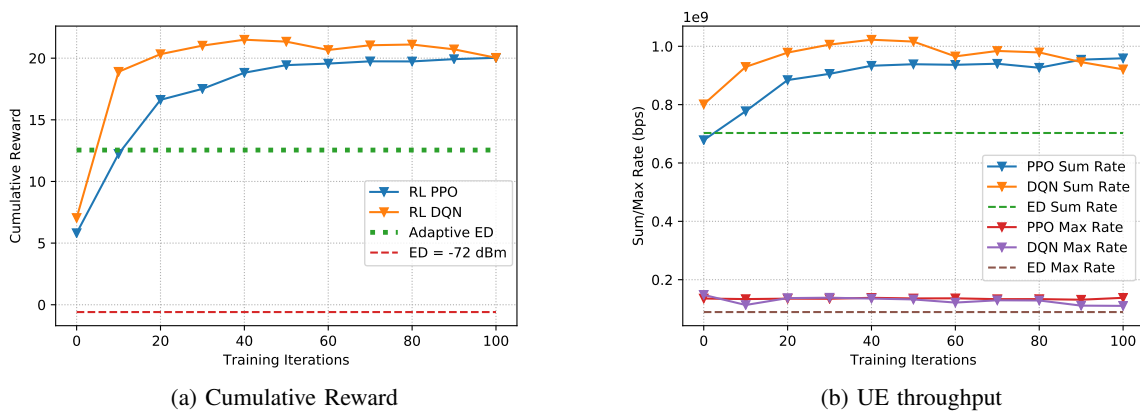


Fig. 8. Results evaluated on Validation Set for UMi-Street Canyon layout.

Rapid Training Convergence and Low Sample Complexity: Since we utilize a *decentralized actor centralized critic* approach for training the NNs deployed at each BS, as described in Section IV-F, we were able to significantly lower the number of training iterations required for the cumulative reward to stabilize, while also lowering the number of training samples needed at each iteration as compared to [20]. For all layouts utilized in this paper, we were able to achieve convergence within 100 iterations with a memory of size $N_{\text{batch}} \times L = 1.6 \times 10^4$ samples at each iteration, while in [20], each layout considered required at least 4000 iterations to achieve training convergence with a memory size of 5×10^5 samples at each iteration.

We now attempt to highlight a few key features of the RL algorithms for adaptive modulation as compared to the traditional ED baselines.

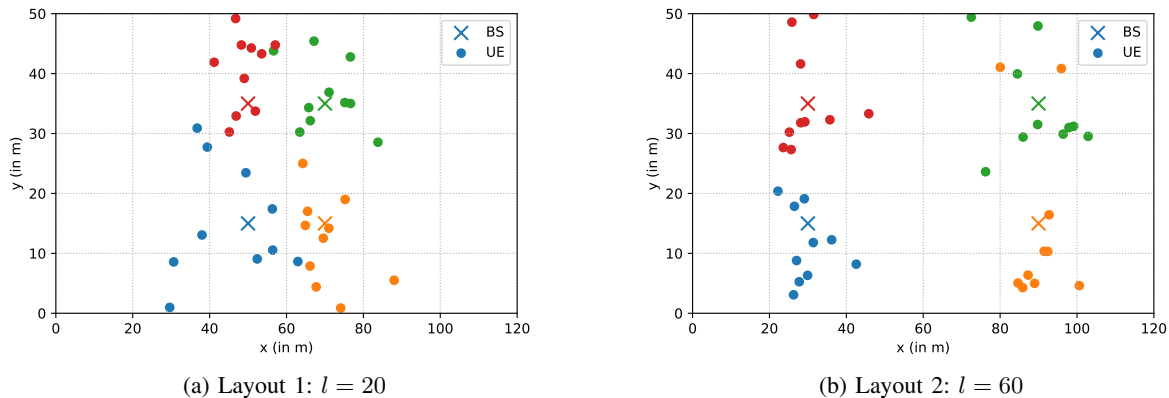


Fig. 9. Two layouts of 4 BS's at the corners of a $l \times 20$ m rectangle.

A. BS separation and UE density

Increased inter-BS separation improves PF metric accumulated: To highlight the impact of the inter-BS separation on the cumulative reward earned, we sample $N = 4$ BSs from the InH-Office layout and their associated UEs, and proceed to train the RL PPO and DQN algorithms on these configurations. As shown in Fig. 9a and 9b respectively, with the increased inter-BS separation in Layout 2, more BSs can transmit simultaneously in Layout 2 as compared to Layout 1. This explains the higher cumulative reward accumulated by all methods - the baselines and the RL algorithm - for Layout 2 in Fig 10b as compared to Layout 1 in 10a.

Higher UE density degrades performance of ED: Another feature evident in Fig. 10 is that the RL algorithms only approaches the Adaptive ED baseline in terms of cumulative reward, in contrast to Fig. 7a and 8a where it significantly outperforms Adaptive ED. A possible explanation for this is that with a larger number of BSs, the same set of ED baselines of -22 to -92 dBm tend to be crossed by $\sum_j \mathcal{E}_{ij}^{\theta_i}$ with only a small fraction of the BSs allowed to transmit. In other words, the ED baselines tend to be overly pessimistic for the realistic InH-Office and UMi-Street Canyon layouts and highlight the need for an RL approach that jointly utilizes UE signalling parameters and BS sensing information to choose a transmit modulation scheme.

B. Modifying inter-BS energy vector $\mathcal{E}_i^{\theta_i}$

Truncating $\mathcal{E}_i^{\theta_i}$ does not impact RL performance: One of the drawbacks of the inter-BS energy vector $\mathcal{E}_i^{\theta_i}$ introduced as part of the CON state in Section III, is that its length equals the number of BSs in the layout. This is clearly not scalable to any practical deployment. However,

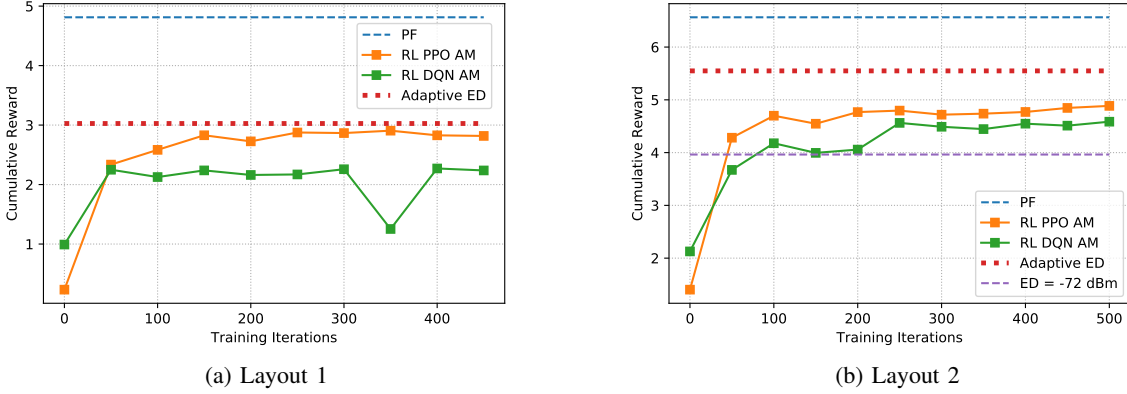


Fig. 10. Cumulative Reward evaluated on Validation Set v/s Training Iterations for *Layout 1* and *Layout 2*. For *Layout 1*, ED = -72 dBm has a reward of -13.29 and has not been shown.

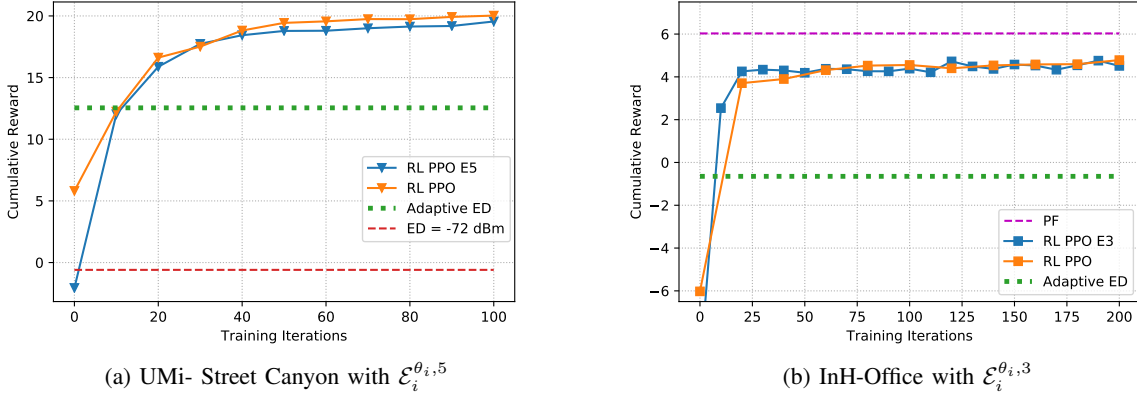


Fig. 11. Cumulative Reward evaluated on Validation Set v/s Training Iterations with fixed length energy vector.

in [20], we provided experimental evidence of the need to preserve the ordering of elements in $\mathcal{E}_i^{\theta_i}$ across agents, such that the CON NNs could assign an identity to the interfering transmitter. Hence we adopt the following strategy - restrict $\mathcal{E}_i^{\theta_i}$ to be of fixed length, not dependent on the number of BSs in the layout. Then append each energy measurement as $\langle j, \mathcal{E}_i^{\theta_{ij}} \rangle$ before inputting to the CON NNs $\pi_i^{\text{CON}} / V_i^{\text{CON}}$. Adding the index j is aimed at informing the NN as to the identity of the interfering BS. The validation results for the UMi Street Canyon layout are shown in Fig. 11a with length of $\mathcal{E}_i^{\theta_{i,5}}$ as 5 for $N = 19$. It should be noted that the 5 entries in $\mathcal{E}_i^{\theta_{i,5}}$ are the 5 largest entries from $\mathcal{E}_i^{\theta_i}$. Similar results are shown for the InH-Office layout with length of $\mathcal{E}_i^{\theta_{i,3}}$ as 3 for $N = 12$. The results indicate that we can use a smaller number of entries in $\mathcal{E}_i^{\theta_i}$ without impacting the policy learnt, improving the practicality of the approach.

VII. CONCLUSION AND FUTURE DIRECTIONS

In this paper, we formulated novel distributed implementations of two single agent RL algorithms - PPO [23] and DQN [12] - adapted to a contention-based medium access *DEC-POMDP* to choose the optimal transmit modulation scheme in each time slot that maximized the long term average throughput for all UEs. Our framework jointly utilized UE signalling parameters such as the signal and interference power from the last time slot in combination with spectrum sensing information from the current time slot to perform rate adaptation in a way that maximized proportional fairness network-wide. We utilized a centralized training procedure with decentralized inference – *decentralized actor centralized critic* – to improve the scalability of our approach, applying our algorithms to both indoor and outdoor layouts of 12 and 19 BSs respectively. The RL algorithms were found to significantly outperform a genie-aided configuration adaptive ED threshold in terms of the PF metric, and also improved the sum and max rates achieved by the UEs.

There are many possible extensions of the framework in this paper. For example, the current formulation assumes all BSs are owned by a single operator and hence are focused on cooperatively maximizing the long term average throughput of the UEs they serve. However, in a practical deployment, each operator (such as AT&T or Verizon) owns a disjoint set of BSs and compete with each other for utilization of the same spectrum. Moreover, real DL transmissions are bursty i.e. the BS does not always have data to transmit and consequently, RL policies at other BSs should be trained to exploit the bursty nature of interfering traffic. Finally, a drawback of our approach is the need to deploy NNs with the same architecture but different weights at each BS. Ideally, we would want to deploy the same NN at each BS, akin to utilizing a common ED threshold at all BSs. With heavy expected application of machine learning algorithms in 6G systems [43], distributed approaches to dynamic spectrum access with rate adaption capabilities and scalability to large networks could be of considerable importance.

REFERENCES

- [1] A. Doshi and J. G. Andrews, “Distributed Proximal Policy Optimization for Contention-Based Spectrum Access,” in *Proc., IEEE Asilomar*, Nov. 2021.
- [2] N. Patriciello, S. Lagén, B. Bojović, and L. Giupponi, “NR-U and IEEE 802.11 Technologies Coexistence in Unlicensed mmWave Spectrum: Models and Evaluation,” *IEEE Access*, vol. 8, pp. 71 254–71 271, Apr. 2020.
- [3] Qualcomm. (2014, Jun.) Qualcomm Research LTE in Unlicensed Spectrum: Harmonious Coexistence With WiFi. [Online]. Available: <https://www.qualcomm.com/media/documents/files/lte-unlicensed-coexistence-whitepaper.pdf>

- [4] 3GPP, “Feasibility Study on Licensed-Assisted Access to Unlicensed Spectrum,” 3rd Generation Partnership Project (3GPP), Technical Report (TR) 36.889, Jul. 2015, version 13.0.0.
- [5] ETSI, “Broadband Radio Access Networks (BRAN); 5GHz high performance RLAN,” European Telecommunications Standards Institute (ETSI), European Standards (EN) 301 893, Jul. 2014, version 1.7.2.
- [6] E. Dahlman, S. Parkvall, and J. Skold, *5G NR: The next generation wireless access technology*. Academic Press, Sep. 2020.
- [7] 3GPP, “NR; Physical layer procedures for data,” 3rd Generation Partnership Project (3GPP), Technical Specification (TS) 38.214, Jan. 2021, version 16.4.0.
- [8] A. Sampath, P. S. Kumar, and J. M. Holtzman, “On setting reverse link target SIR in a CDMA system,” in *1997 IEEE 47th Vehicular Technology Conference. Technology in Motion*, vol. 2. IEEE, May 1997, pp. 929–933.
- [9] J. P. Leite, P. H. P. de Carvalho, and R. D. Vieira, “A flexible framework based on reinforcement learning for adaptive modulation and coding in OFDM wireless systems,” in *Proc., IEEE Wireless Networking and Comm. Conf.*, Apr. 2012, pp. 809–814.
- [10] P. H. Portela de Carvalho, R. D. Vieira, and J. P. Leite, “A Continuous-State Reinforcement Learning Strategy for Link Adaptation in OFDM Wireless Systems,” *Journal of Communication and Information Systems*, vol. 30, no. 1, pp. 47–57, Jun. 2015.
- [11] R. Bruno, A. Masaracchia, and A. Passarella, “Robust adaptive modulation and coding (AMC) selection in LTE systems using reinforcement learning,” in *Proc., IEEE Veh. Technology Conf.*, Sep. 2014, pp. 1–6.
- [12] V. Mnih, K. Kavukcuoglu, D. Silver, A. A. Rusu, J. Veness, M. G. Bellemare, A. Graves, M. Riedmiller, A. K. Fidjeland *et al.*, “Human-level control through deep reinforcement learning,” *Nature*, vol. 518, no. 7540, pp. 529–533, Feb. 2015.
- [13] L. Zhang, J. Tan, Y.-C. Liang, G. Feng, and D. Niyato, “Deep reinforcement learning-based modulation and coding scheme selection in cognitive heterogeneous networks,” *IEEE Trans. on Wireless Communications*, vol. 18, no. 6, pp. 3281–3294, Jun. 2019.
- [14] M. P. Mota, D. C. Araujo, F. H. C. Neto, A. L. de Almeida, and F. R. Cavalcanti, “Adaptive Modulation and Coding based on Reinforcement Learning for 5G Networks,” in *2019 IEEE Globecom Workshops (GC Wkshps)*, Dec. 2019, pp. 1–6.
- [15] J. Lundén, V. Koivunen, S. R. Kulkarni, and H. V. Poor, “Reinforcement learning based distributed multiagent sensing policy for cognitive radio networks,” in *IEEE Intl. Symposium on Dynamic Spectrum Access Networks (DySPAN)*, May 2011, pp. 642–646.
- [16] O. Naparstek and K. Cohen, “Deep multi-user reinforcement learning for distributed dynamic spectrum access,” *IEEE Trans. on Wireless Communications*, vol. 18, no. 1, pp. 310–323, Nov. 2018.
- [17] M. Tonnemacher, C. Tarver, J. Cavallar, and J. Camp, “Machine Learning Enhanced Channel Selection for Unlicensed LTE,” in *IEEE Intl. Symposium on Dynamic Spectrum Access Networks (DySPAN)*, Nov. 2019, pp. 1–10.
- [18] M. Tonnemacher, C. Tarver, V. Chandrasekhar, H. Chen, P. Huang, B. L. Ng, J. C. Zhang, J. R. Cavallaro, and J. Camp, “Opportunistic channel access using reinforcement learning in tiered CBRS networks,” in *IEEE Intl. Symposium on Dynamic Spectrum Access Networks (DySPAN)*, Oct. 2018, pp. 1–10.
- [19] N. Naderializadeh, J. Sydir, M. Simsek, and H. Nikopour, “Resource management in wireless networks via multi-agent deep reinforcement learning,” *IEEE Trans. on Wireless Communications*, Jan. 2021.
- [20] A. Doshi, S. Yerramalli, L. Ferrari, T. Yoo, and J. G. Andrews, “A Deep Reinforcement Learning Framework for Contention-Based Spectrum Sharing,” *IEEE Journal on Sel. Areas in Communications*, vol. 39, no. 8, pp. 2526–2540, Jun. 2021.
- [21] J. Smith, “Odd-bit quadrature amplitude-shift keying,” *IEEE Trans. on Communications*, vol. 23, no. 3, pp. 385–389, Mar. 1975.

- [22] J. Foerster, I. A. Assael, N. De Freitas, and S. Whiteson, "Learning to communicate with deep multi-agent reinforcement learning," in *Adv. in Neural Info. Process. Systems*, May 2016, pp. 2137–2145.
- [23] J. Schulman, F. Wolski, P. Dhariwal, A. Radford, and O. Klimov, "Proximal policy optimization algorithms," *CoRR*, vol. abs/1707.06347, Jul. 2017.
- [24] 3GPP, "Study on NR-based access to unlicensed spectrum," 3rd Generation Partnership Project (3GPP), Technical Report (TR) 38.889, Dec. 2018, version 16.0.0.
- [25] A. Lozano and N. Jindal, "Transmit diversity vs. spatial multiplexing in modern MIMO systems," *IEEE Trans. on Wireless Communications*, vol. 9, no. 1, pp. 186–197, Jan. 2010.
- [26] F. P. Kelly, A. K. Maulloo, and D. K. Tan, "Rate control for communication networks: shadow prices, proportional fairness and stability," *Journal of the Operational Research society*, vol. 49, no. 3, pp. 237–252, Mar. 1998.
- [27] B. Wang and D. Zhao, "Scheduling for long term proportional fairness in a cognitive wireless network with spectrum underlay," *IEEE Trans. on Wireless Communications*, vol. 9, no. 3, pp. 1150–1158, Mar. 2010.
- [28] R. S. Sutton and A. G. Barto, *Reinforcement learning: An introduction*. MIT press, Oct. 2018.
- [29] A. Tampuu, T. Matiisen, D. Kodelja, I. Kuzovkin, K. Korjus, J. Aru, J. Aru, and R. Vicente, "Multiagent cooperation and competition with deep reinforcement learning," *PloS one*, vol. 12, no. 4, Apr. 2017.
- [30] Y. Shoham and K. Leyton-Brown, *Multiagent systems: Algorithmic, game-theoretic, and logical foundations*. Cambridge University Press, 2008.
- [31] E. Zawadzki, A. Lipson, and K. Leyton-Brown, "Empirically Evaluating Multiagent Learning Algorithms," *CoRR*, vol. abs/1401.8074, Jan. 2014.
- [32] R. J. Williams, "Simple statistical gradient-following algorithms for connectionist reinforcement learning," *Machine learning*, vol. 8, no. 3-4, pp. 229–256, May 1992.
- [33] J. Schulman, P. Moritz, S. Levine, M. Jordan, and P. Abbeel, "High-dimensional continuous control using generalized advantage estimation," *Proc. ICLR*, Jun. 2015.
- [34] J. Schulman, S. Levine, P. Abbeel, M. Jordan, and P. Moritz, "Trust region policy optimization," in *International conference on machine learning*. PMLR, Jun. 2015, pp. 1889–1897.
- [35] M. Hausknecht and P. Stone, "Deep Recurrent Q-learning for Partially Observable MDPs," in *AAAI Fall Symposium Series*, Sep. 2015.
- [36] S. Hochreiter and J. Schmidhuber, "Long short-term memory," *Neural computation*, vol. 9, no. 8, pp. 1735–1780, Nov. 1997.
- [37] R. Lowe, Y. Wu, A. Tamar, J. Harb, O. Pieter Abbeel, and I. Mordatch, "Multi-agent actor-critic for mixed cooperative-competitive environments," in *Adv. in Neural Info. Process. Systems*, vol. 30, Jun. 2017.
- [38] 3GPP, "Study on channel model for frequencies from 0.5 to 100 GHz," 3rd Generation Partnership Project (3GPP), Technical Report (TR) 38.901, Jan. 2020, version 16.1.0.
- [39] X. Zhang, H. Yu, and G. Wei, "Exact symbol error probability of cross-QAM in AWGN and fading channels," *EURASIP Journal on Wireless Communications and Networking*, vol. 2010, pp. 1–1, Dec. 2010.
- [40] Z. Wang, T. Schaul, M. Hessel, H. Hasselt, M. Lanctot, and N. Freitas, "Dueling network architectures for deep reinforcement learning," in *Intl. Conf. on Machine Learning (ICML)*, Jun. 2016, pp. 1995–2003.
- [41] D. P. Kingma and J. Ba, "Adam: A method for stochastic optimization," in *Proc. ICLR*, Dec. 2014.
- [42] A. Goldsmith, *Wireless communications*. Cambridge university press, 2005.
- [43] S. Dang, O. Amin, B. Shihada, and M.-S. Alouini, "What should 6G be?" *Nature Electronics*, vol. 3, no. 1, pp. 20–29, Jan. 2020.